Transfer hydrogenation from glycerol over a Ni-Co/CeO2 catalyst: A highly efficient and sustainable route to produce lactic acid

Tang, Zhenchen; Cao, Huatang; Tao, Yehan; Heeres, Hero J.; Pescarmona, Paolo P.

Published in:
Applied Catalysis B: Environmental

DOI:
10.1016/j.apcatb.2019.118273

Publication date:
2020

Applied Catalysis B: Environmental 263 (2020) 118273

Contents lists available at ScienceDirect

Applied Catalysis B: Environmental

journal homepage: www.elsevier.com/locate/apcatb

Transfer hydrogenation from glycerol over a Ni-Co/CeO_2 catalyst: A highly efficient and sustainable route to produce lactic acid

Zhenchen Tang[a], Huatang Cao[b], Yehan Tao[a], Hero J. Heeres[a], Paolo P. Pescarmona[a,*]

[a] Chemical Engineering Group, Engineering and Technology Institute Groningen, University of Groningen, Nijenborgh 4, 9747 AG Groningen, the Netherlands
[b] School of Materials, University of Manchester, Manchester M139PL, United Kingdom

ARTICLE INFO

Keywords:
Glycerol
Lactic acid
Ni catalyst
Co catalyst
Alloy effects
Transfer hydrogenation

ABSTRACT

Bimetallic Ni-Co catalysts supported on nanosized CeO_2 were prepared and investigated as heterogeneous catalysts for the transfer hydrogenation between glycerol and various H_2 acceptors (levulinic acid, benzene, nitrobenzene, 1-decene, cyclohexene) to selectively produce lactic acid (salt) and the target hydrogenated compound. The bimetallic NiCo/CeO_2 catalyst showed much higher activity than the monometallic Ni or Co counterparts (with equal total metal mass), thus indicating strong synergetic effects. The interaction between the metallic sites and the CeO_2 support was thoroughly characterised by means of transmission electron microscopy (TEM), scanning transmission electron microscopy (STEM), energy-dispersive X-ray spectroscopy (EDX) mapping, X-ray photoelectron spectroscopy (XPS), hydrogen-temperature programmed reduction (H_2-TPR) and X-ray diffraction (XRD). Combining characterisation and catalytic results proved that the Ni species are intrinsically more active than Co species, but that incorporating Co into the catalyst formulation prevented the formation of large Ni particles and led to highly dispersed metal nanoparticles on CeO_2, thus leading to the observed enhanced activity for the bimetallic system. The highest yield of lactic acid (salt) achieved in this work was 93% at 97% glycerol conversion (160 °C, 6.5 h at 20 bar N_2, NaOH: glycerol = 1.5). The NiCo/CeO_2 catalyst also exhibited high activity and selectivity towards the target hydrogenated products in the transfer hydrogenation reactions between glycerol and various H_2 acceptors. Batch recycle experiments showed good reusability, with retention of 80% of the original activity after 5 runs.

1. Introduction

Biomass represents a sustainable alternative carbon source compared to fossil resources like oil, gas and coal [1–3]. Considering the limited reserves of these fossil resources, growing research efforts are being devoted to the development of efficient catalytic systems for biomass valorisation into biofuels and biobased chemicals [1,3,4]. For the upgrading of biobased compounds into valuable chemicals, metallic catalysts are often required for one or more step(s) in a multi-step reaction that may involve hydrogenation, oxidation and/or hydrogenolysis [3,4]. On one hand, noble metal catalysts, such as Au, Pt, Pd and Ru nanoparticles, often exhibit excellent catalytic performance in specific reactions [3]; on the other hand, their high cost limits the extension of their application from lab-scale to the industry. Moreover, these catalysts often suffer from stability issues since the nanoparticles tend to aggregate and thus decrease their activity under hydrothermal reaction conditions [4,5]. As such, there is a strong need for developing noble-metal-free catalysts, which ideally should have comparable performance and better stability compared to those noble metal catalysts [3]. Among the biobased compounds that typically require the use of noble metal catalysts for their oxidation, glycerol is an attractive platform molecule [6,7]. It is produced in large amounts (above 1 million tons crude glycerol in 2016) as the major side product from the biodiesel industry by transesterification of vegetable oils with methanol [4,8]. This led to an oversupply of glycerol and, therefore, has prompted both academia and industry to develop efficient catalytic routes to convert it into several valuable chemical products [9–11]. Lactic acid and alkyl lactates can be produced from glycerol through a dehydrogenation-rearrangement pathway (Scheme 1) [8,12–14]. Lactic acid has a wide range of applications, including that as monomer of poly-lactic acid, a biodegradable bio-polymer with various applications in the food, pharmaceutical and packaging industry [12]. Currently, lactic acid is produced by fermentation of carbohydrates, which generates large amounts of salts in the product work-up section and has a relatively low volumetric production rate [15,16]. The chemocatalytic route involving the dehydrogenation of glycerol and consecutive

* Corresponding author.
E-mail address: p.p.pescarmona@rug.nl (P.P. Pescarmona).

https://doi.org/10.1016/j.apcatb.2019.118273
Received 24 May 2019; Received in revised form 30 August 2019; Accepted 8 October 2019
Available online 14 October 2019

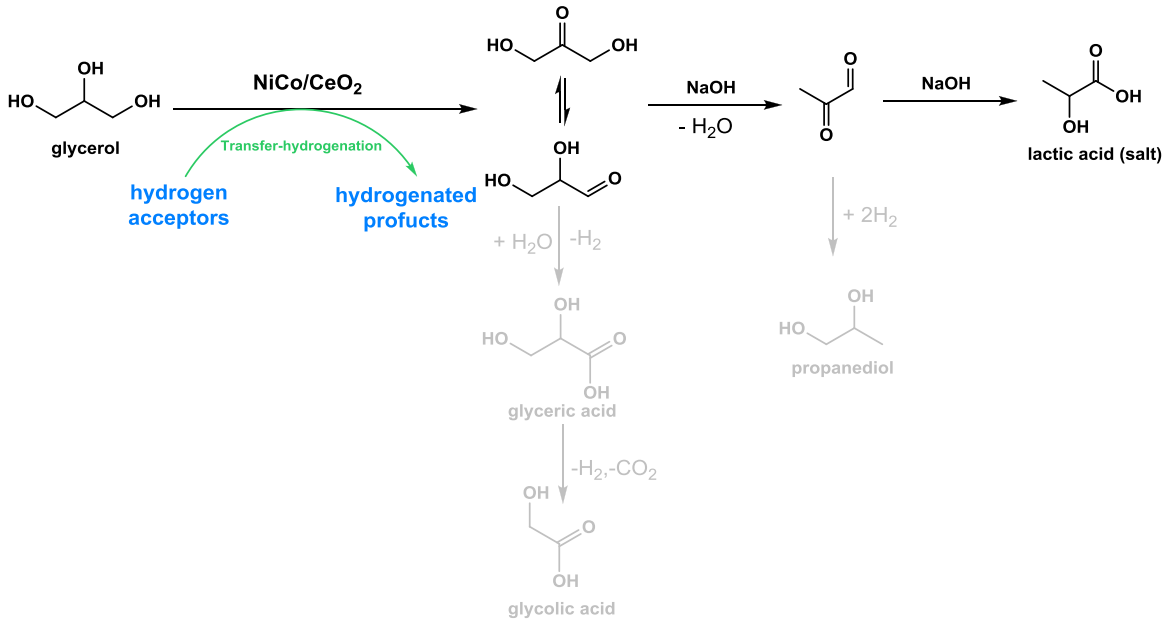

Scheme 1. Catalytic route from glycerol to lactic acid and from a hydrogen acceptor (cyclohexene, levulinic acid, benzene, nitrobenzene or 1-decene) to the corresponding hydrogenated product with inter-molecular transfer hydrogenation.

rearrangement of the triose intermediates (Scheme 1) is considered a viable, sustainable alternative to the fermentation process [12]. This chemocatalytic route implies a nominal formation of H_2 and in this sense can be correlated to the use of glycerol as feedstock for the sustainable production of H_2 through aqueous-phase reforming (APR) [7,11,17]. Hydrogen is widely used in current chemical industry (e.g. ammonia synthesis, Fischer-Tropsch process, steel industry and various hydrogenation reactions) and in the power fuel cell systems as a clean power source [2,11,18]. Clearly, routes that allow producing H_2 from a renewable source such as biomass represent a sustainable alternative to the current production through methane steam reforming, which is based on a fossil resource and requires extremely harsh conditions [2,19].

The conversion of glycerol into lactic acid requires metallic sites for the first step, i.e. the dehydrogenative oxidation, and a base or a combination of Brønsted and Lewis acid sites for the second step (Scheme 1). Most studies used noble metal catalysts for the first step, such as Pt, Pd, Au and their alloys [12,20–22]. Pt/C was used for the hydrogenolysis of glycerol under He atmosphere and gave 55% selectivity to lactic acid at 95% conversion of glycerol [23,24]. Supported Au and its alloy catalysts ($AuPt/TiO_2$) were firstly used with O_2 as the oxidant, reaching 30% glycerol conversion and 86% selectivity to lactic acid at 90 °C [21]. The first report of a bifunctional catalyst for the conversion of glycerol into lactic acid without adding a base employed Pt supported on a zeolite (Sn-MFI) and achieved an excellent 81% selectivity towards lactic acid at 90% conversion of glycerol under O_2 (6 bar) at a relatively mild temperature (90 °C) [14]. Catalysts based on non-noble transition metals, such as Ni, Co and Cu, were also found to be active in converting glycerol to lactic acid under inert atmosphere in the presence of a base [20,25–29]. A Ni/graphite catalyst tested at 250 °C for 2 h yielded 89% lactic acid at full glycerol conversion [20]. A series of $30\%CuO/ZrO_2$ catalysts were also developed and reached 95% yield of lactic acid at 200 °C [29]. A recent study reported a $20\%Co_3O_4/CeO_2$ catalyst that achieved 80% selectivity to lactic acid with 85% glycerol conversion at 250 °C for 8 h [27]. All these non-noble metal catalysts were employed in the presence of a homogeneous base (NaOH) and at relatively high reaction temperatures (200–250 °C), under which conditions the base alone would display a significant activity in the conversion of glycerol to lactic acid [30,31]. An additional drawback of the Ni, Cu and Co-based systems is the high metal-to-glycerol ratio that was needed to achieve acceptable reaction rates. Moreover, the Cu and Co-based catalysts suffered remarkable loss of activity upon reuse, probably due to leaching of metal species under the hydrothermal conditions [27,29]. If the conversion of glycerol to lactic acid (salt) is carried out under inert atmosphere, the initial dehydrogenative oxidation step (Scheme 1) nominally liberates one molecule of H_2 per molecule of glycerol [14,25]. However, the hydrogen generated in such system is highly diluted by N_2 in most cases and is thus difficult to collect. In this context, it is more attractive to utilise *in-situ* the hydrogen removed from glycerol in the reduction of relevant target compounds. Here, we report a bimetallic Ni-Co catalyst supported on CeO_2 with remarkably high activity in the transfer hydrogenation between glycerol and several H_2 acceptors, under relatively mild hydrothermal conditions (160 °C) and in the presence of NaOH as promotor. The choice of investigating a Ni-based catalyst was inspired by the above-mentioned activity of this metal in converting glycerol to lactic acid, combined with its well-known activity in catalysing hydrogenation reactions as significantly cheaper alternative to noble metals (e.g. Pt and Pd) [3,32]. The idea of using Ni in a bimetallic system was justified by previous reports that showed that the catalytic performance of Ni could be enhanced by incorporating another component, such as Co or Cu, which led to stronger metal-support interaction with consequent smaller metal particle size [3,4,33]. Namely, bimetallic Ni-based catalysts supported on ZrO_2 showed much better performance in the dry reforming of methane (Ni-Co) or in the oxidative steam reforming of methanol (Ni-Cu) compared to their monometallic counterparts [34–36]. In this work, different oxides were tested as support for the Ni-based catalysts, with CeO_2 leading to the highest activity in glycerol conversion. Our bimetallic Ni-Co catalytic system was also compared to its monometallic counterparts, showing higher activity and allowing to reach very high conversion of glycerol with excellent selectivity towards lactic acid, and to combine this reaction with the efficient hydrogenation of several unsaturated compounds in a one-pot process.

2. Experimental section

2.1. Reactants and materials

Glycerol (99%), 1,3-dihydroxyacetone dimer (97%), glyceraldehyde

(90%), glycolic acid (99%), lactic acid (98%), pyruvic aldehyde (40 wt % in H_2O), cyclohexene (99%), cyclohexane (99.5%), sodium hydroxide (98%), benzene (99.9%), levulinic acid (99%), 4-hydroxypentanoic acid, γ-valerolactone (99%), nickel(II) nitrate hexahydrate (98.5%), cobalt(II) nitrate hexahydrate (98%), copper(II) nitrate hemi (pentahydrate) (98%), titanium oxide (P25), magnesium oxide (99%) cerium oxide (nanopowder, nominally < 25 nm, though some large particles were observed by TEM; this compound is denoted as CeO_2 for the sake of simplicity, though it contains both Ce^{IV} and Ce^{III} and it is thus actually CeO_{2-x}), zirconium oxide (nanopowder, < 100 nm) were purchased from Sigma Aldrich. Glyceric acid (20 wt% in H_2O), nitrobenzene (99.5%), aniline (98%), azobenzene (98%), azoxybenzene (98%) were purchased from TCI Chemicals. Active carbon Norit SX1G was purchased from Cabot. The H_2O used in this work was always of MilliQ grade. All chemicals were used without further purification.

2.2. Catalyst synthesis

A wet impregnation method was used for the preparation of catalysts based on Ni, Co, Cu, NiCo, NiCu supported on CeO_2 and ZrO_2. Typically, CeO_2 (2 g) was mixed with an aqueous solution of $Ni(NO_3)_2$ or $Co(NO_3)_2$ or $Cu(NO_3)_2$ or the combination of two of them (2 M, with the volume of the solution being defined by the target loading of Ni, Co and Cu). The slurry was stirred at room temperature until the water evaporated. The solid mixture was then dried at 100 °C overnight. The resulting solids were milled to fine powder and then calcined at 550 °C in the oven under static air (heating rate 3 °C/min). The calcined catalysts were further reduced in a tube oven under H_2 flow (99.9% and 200 mL/min) at 400 °C (heating rate 3 °C/min) for 2 h. The gas flow was switched to N_2 for 1 h to wipe away the adsorbed H_2 on the catalyst surface before taking the catalyst out from the tube oven. A typical reduced catalyst prepared by this method was named as $10NiCo/CeO_2$, in which 10 stands for the total loading of Ni and Co (wt%), in which the mass ratio between Ni and Co is always kept as 1:1. In addition, as a reference, the catalyst was also used directly after calcination at 550 °C without further reduction in H_2, which was named as $10NiCo/CeO_2$-C.

2.3. Catalytic tests

The catalytic experiments were carried out in a 100 mL Parr stainless steel autoclave reactor equipped with a Teflon liner and an overhead stirrer. In a typical test, a predetermined amount of the catalyst together with a mixture of aqueous solution of glycerol (0.5 M in 20 mL), NaOH (0.15 mol) and the selected hydrogen acceptor (0.2 mol, as organic phase) were loaded into the reactor. The reaction was performed under N_2 (20 bar) for 4.5 h at 160 °C (extra heating time 0.5 h) at a stirring speed of 800 rpm. Next, the reactor was depressurised and the reaction content (in two phases) was taken separately and filtered to remove the catalyst. The organic phase was analysed by gas chromatography using a Thermo Trace GC equipped with a Restek Stabilwax-DA column (30 m × 0.32 mm × 1 μm) and a FID detector. The aqueous phase was first neutralised and diluted by H_2SO_4 (1 M), then analysed by high performance liquid chromatography (HPLC, Agilent Technologies 1200 series, Bio-Rad AminexHPX-87H 300 × 7.8 mm column) at T = 60 °C, with 0.5 mM H_2SO_4 as eluent (flow rate: 0.55 mL/min) using a combination of refractive index detector and ultra-violet detector. For the analysis of nitrobenzene and its products, conversion and selectivity were determined by GC analysis using an Agilent Technologies 7980B GC equipped with an Agilent DB-5#6 (5%-Phenyl)-methylpolysiloxane column (15 m, 320 μm ID). The identification of the products was performed by GC-mass spectrometry (GC–MS) on an HP 6890 Series GC equipped with a Restek Rxi-5Si MS fused silica column (30 m, 250 μm ID) coupled to an HP 5973 Mass Selective Detector. Each component was calibrated using solutions of the individual components at 4 different concentrations.

For the catalyst recycle tests, a small amount of the reaction mixture was collected for analysis, the remaining mixture was filtered and the catalyst was recovered. The catalyst was washed first with H_2O (20 mL), then with ethanol (20 mL), and this procedure was repeated 3 times, after which the solid was dried overnight at 100 °C. This solid was used for another batch experiment.

2.4. Characterisation of the catalysts

Transmission electron microscopy (TEM), scanning transmission electron microscopy (STEM) and energy-dispersive X-ray spectroscopy (EDX) mapping measurements were performed on a FEI Tecnai T20 electron microscope operating at 200 keV with an Oxford Xmax 80 T detector. The samples were prepared by ultra-sonication in ethanol followed by drop-casting of the material on a copper grid.

Nitrogen physisorption isotherms were measured at −196 °C using a Micromeritics ASAP 2420 apparatus. The Brunauer-Emmet-Teller (BET) method was used to calculate the specific surface area. The Barrett-Joyner-Halenda (BJH) method was used to calculate the pore volume.

Inductively-coupled plasma optical emission spectrometry (ICP-OES) was performed using a Perkin Elmer Optima 7000 DV instrument in order to obtain the actual metal loadings on the supports.

X-ray photoelectron spectroscopy (XPS) was measured by mounting the catalysts on a conductive tape adhered to the XPS sample holder. No further treatment was carried out prior to the XPS measurement. Then, the sample was loaded into the load lock and the pressure was reduced below $1{\cdot}10^{-7}$ mbar. The XPS measurements were performed using a Surface Science SSX-100 ESCA instrument equipped with a monochromatic Al Kα X-ray source ($h\nu$ = 1486.6 eV). During the measurement, the pressure was kept below $2{\cdot}10^{-9}$ mbar in the analysis chamber. For acquiring the data, a spot size with a 600 μm diameter was used. The neutraliser was on to avoid charging effects. All XPS spectra were analysed using the Winspec software package developed by LISE laboratory, University of Namur, Belgium, including Shirley background subtraction and peak deconvolution.

Hydrogen-temperature programmed reduction (H_2-TPR) measurements were performed on an Autochem II 2920 from Micromeritics. In a typical experiment, 80 mg of sample was pre-treated at 500 °C (heating rate 10 °C/min) for 1 h in a flow of He (30 mL/min). Subsequently, the sample was cooled down to 50 °C under the same flow of He. The reduction analysis was performed from 50 to 900 °C (10 °C/min) in a 30 mL/min flow of 5 vol.% H_2 in He.

X-ray diffraction (XRD) measurements were performed on a D8 Advance Bruker diffractometer with a CuKα 1 radiation (λ = 1.5418 Å). The XRD patterns were collected under 40 kV and 40 mA in the range of 10-80°.

Definitions:

The glycerol conversion (Conv./%) is defined by Eq. (1):

$$\text{Conv.}=\frac{C_{(g,0)}-C_{(g)}}{C_{(g,0)}}\times 100\% \quad (1)$$

in which $C_{(g)}$ is the molar concentration of glycerol after a certain reaction time and $C_{(g,0)}$ is the initial concentration of glycerol.

Product selectivity for a compound P is defined by Eq. (2):

$$S_p = \frac{C_{(p)}}{C_{(g,0)}-C_{(g)}}\times 100\% \quad (2)$$

in which $C_{(p)}$ is the molar concentration of a product after a certain reaction time.

The yield of transfer hydrogenation is defined by Eq. (3):

$$Y_{\text{trans}-H} = \frac{\sum (x^{*}n_{(p1)})}{n_{(g,0)}-n_{(g)}}\times 100\% \quad (3)$$

in which x is the number of hydrogen atoms needed for the reduction of product 1, $n_{(p1)}$ is the molar amount of product 1, $n_{(g)}$ is the

Table 1
Catalytic performance of Ni catalysts supported on activated carbon and various metal oxides.

Entry	Catalyst	Conv.$_{GLY}$ (%)	Y_{LA} (%)	$S_{(transfer-H)}$ (%)	Selectivity in the conversion of glycerol (%)				Yield in the conversion of cyclohexene (%)[a]	
					Lactic acid	Glyceric acid	Glycolic acid	Propanediol	Cyclohexane	Benzene
1	10Ni/AC	22	21	42	97	0	0	0.2	5.5	0.5
2	10Ni/MgO	6.2	5.7	42	91	0	0.1	0.2	1.4	0.1
3	10Ni/TiO_2	14	13	29	98	0	0	0	2.4	0.2
4	10Ni/ZrO_2	63	60	33	95	1.2	0	3.1	10	0
5	10Ni/CeO_2	53	52	20	98	0	0	2.0	5.3	0.1

Reaction conditions: aqueous glycerol solution: 10 mmol (0.5 M, 20 mL); cyclohexene: 20 mmol; Ni catalyst: 0.1 g; NaOH: 15 mmol; temperature: 160 °C; reaction time: 4.5 h; N_2 pressure: 20 bar.

[a] Under the employed reaction conditions ($mol_{glycerol}$: $mol_{cyclohexene}$ = 1 : 2) the maximum theoretical yield of cyclohexane is 50%.

molar amount of glycerol after a certain reaction time and $n_{(g,0)}$ is the initial molar amount of glycerol.

The term "lactic acid" is used in this article to describe the product obtained from the reaction mixture, which is actually sodium lactate (mixed with a small portion of lactic acid from hydrolysis).

3. Results and discussion

3.1. Preliminary screening of supports and metals

Our study of the conversion of glycerol into lactic acid coupled with the transfer hydrogenation to an unsaturated compound started with the investigation of the catalytic behaviour of Ni catalysts (10 wt%) as a function of the type of the material (activated carbon (AC) and various metal oxides) on which the metal particles were supported by wet impregnation. The five catalysts were tested at 160 °C in the presence of NaOH as promotor and using a model compound as cyclohexene as the H_2 acceptor (Table 1). Ni supported on AC, MgO and TiO_2 showed relatively low activity (entries 1–3, Table 1), whereas the activity was significantly higher when nanosized CeO_2 and nanosized ZrO_2 were used as support for Ni (glycerol conversion 53% and 63%, respectively; entry 4–5, Table 1), in line with previous reports on other (de)hydrogenation reactions [4,33]. In all cases, high selectivity towards lactic acid (> 91%) was observed. This is attributed to the presence of NaOH, which effectively promotes the deprotonation of glycerol and catalyses the successive isomerisation of the intermediates (glyceraldehyde and dihydroxyacetone) into the lactic acid salt (Scheme 1), thus granting very high selectivity towards the desired product [21,22,28,37]. Small amounts of glyceric acid, glycolic acid and propanediol were detected as side products (Table 1). Glyceric acid is formed through the further dehydrogenation of glyceraldehyde and glycolic acid probably originates from oxidative C−C bond cleavage of glyceric acid [13]. Propanediol (as a mixture of 1,2- and 1,3-isomers) probably forms via the hydrogenolysis of glycerol [38–40]. In addition, for all reactions, very minor amounts of glyceraldehyde and propanoic acid were observed as side products, with selectivity below 0.2% for each of them.

Based on this preliminary study, CeO_2 and ZrO_2 were selected as supports for further study of Ni-based catalysts. Then, we aimed at improving the catalytic performance by incorporating another metallic component, i.e. Co or Cu [3,4,33]. The activity of the bimetallic catalysts was compared to the monometallic counterparts (Table 2), while keeping the total loading of metal at 10 wt% (and with 1:1 mass ratio for the bimetallic systems). The incorporation of Co into the catalyst formulation was highly beneficial when CeO_2 was used as support (10NiCo/CeO_2), leading to 91% glycerol conversion (entry 1, Table 2) compared to 53% conversion obtained over 10Ni/CeO_2 and 46% conversion over 10Co/CeO_2 (entry 5, Table 2). Also the incorporation of Cu enhanced the activity compared to the monometallic counterparts, though the effect was less marked (compare entry 2 in Table 2 to entry 5 in Table 1 and entry 6 in Table 2). On the other hand, the 10NiCo/ZrO_2 catalyst showed almost the same activity as the monometallic 10Ni/ZrO_2, (compare entry 3 in Table 2 with entry 4 in Table 1), whereas the incorporation of Cu proved more beneficial when ZrO_2 was the support, reaching 80% glycerol conversion (entry 4, Table 2). These results indicate a complex interplay between the type of metals and the supports. The benefit brought about by the bimetallic formulation will be elucidated further in the case of the optimum catalyst, i.e. 10NiCo/CeO_2 (vide infra). In all these tests, the selectivity towards lactic acid remained very high (94–96%). Glyceric acid, glycolic acid and propanediol were detected as the main side products, with selectivity < 6% in total. Though the incorporation of Cu enhanced the activity of the Ni-based catalysts, leaching of metal species was observed in the basic medium under hydrothermal conditions, with significant amount of brown Cu-containing precipitate deposition on the stirring bar and reactor walls [28,33,41–43]. Therefore, 10NiCo/CeO_2 was selected for further investigation aimed both at a deeper evaluation of the catalytic performance and at understanding the relationship between structure and catalytic behaviour.

3.2. Characterisation of the NiCo/CeO_2 catalysts

The catalysts presented in this work were prepared by wet impregnation, followed by calcination and finally reduction by H_2. The actual loading of Ni and/or Co determined by ICP-OES (Table 3) was found to be very close to the nominal 10 wt% loading. In the bimetallic Ni-Co catalyst, the actual loading of Ni and Co is 5.6 wt% for both metals, which is slightly higher than the theoretical 5 wt%. The BET surface area was measured before and after loading Ni and Co, showing only a slight decrease (from 32 to 28 m^2/g) compared to the fresh CeO_2 support.

To investigate the possible organisation of Ni, Co and Ni-Co species in crystalline phases on the CeO_2 support, the catalysts were further characterised by XRD before and after reduction (Fig. 1). The materials before reduction (Fig. 1A) display the characteristic peaks of the CeO_2 support together with the typical peaks of NiO (in 10Ni/CeO_2-C) or Co_3O_4 (in 10Co/CeO_2-C) [34,35,44]. The bimetallic 10NiCo/CeO_2-C shows a broad peak at 36.7°, which is slightly shifted compared to the Co_3O_4 peak (37°) and has been attributed to the mixed oxide $NiCo_2O_4$ [34,45–47]. After reduction at 400 °C in H_2 flow, besides the peaks of the CeO_2 support, only one peak at 44.7° belonging to metallic Ni can be seen in the pattern of 10Ni/CeO_2 (Fig. 1B). On the other hand, no signals stemming from Co and/or Ni phases were observed in 10Co/CeO_2 and 10NiCo/CeO_2. These results suggest that relatively large crystalline Ni particles formed upon reduction in 10Ni/CeO_2, while the Co or Ni-Co species obtained after reduction were highly dispersed in the other two catalysts [45–48].

To achieve deeper insight on the dispersion of Ni, Co and bimetallic Ni-Co catalysts supported on nanosized CeO_2, TEM and STEM-EDX-mapping were used to investigate the average size of these metallic domains (Figure S1, 2 and 3). Since the atomic mass of cerium is much higher than that of nickel or cobalt, it is hard to determine the particle size of Ni, Co or Ni-Co alloy on the CeO_2 support based on TEM pictures

Table 2
Catalytic performance of Ni, Co, Cu and bimetallic Ni catalysts supported on CeO_2 and ZrO_2.

Entry	Catalyst	Conv.$_{GLY}$ (%)	Y_{LA} (%)	$S_{(transfer-H)}$ (%)	Selectivity in the conversion of glycerol (%)				Yield in the conversion of cyclohexene (%)[a]	
					Lactic acid	Glyceric acid	Glycolic acid	Propanediol	Cyclohexane	Benzene
1	10NiCo/CeO_2	91	85	24	94	0.8	0	3.2	11	0.4
2	10NiCu/CeO_2	62	59	26	94	0.5	0.5	1.6	8.7	0.4
3	10NiCo/ZrO_2	62	60	15	96	0.8	0.5	2.5	4.9	0.2
4	10NiCu/ZrO_2	80	76	24	95	1.0	0.7	2.5	9.9	0.2
5	10Co/CeO_2	46	43	31	95	3.6	0.6	1.2	7.9	0.3
6	10Cu/CeO_2	44	41	23	95	1.0	0.3	0	4.8	0

Reaction conditions: aqueous glycerol solution: 10 mmol (0.5 M, 20 mL); cyclohexene: 20 mmol; catalyst: 0.1 g; NaOH: 15 mmol; temperature: 160 °C; reaction time: 4.5 h; N_2 pressure: 20 bar.

[a] Under the employed reaction conditions ($mol_{glycerol}$: $mol_{cyclohexene}$ = 1 : 2) the maximum theoretical yield of cyclohexane is 50%. The weight ratio between Ni and (Co or Cu) in the bimetallic catalysts is 1:1.

Table 3
Elemental composition and specific surface area of CeO_2 and Ni, Co, Ni-Co catalysts supported on CeO_2.

Entry	Catalyst	Ni loading/%	Co loading/%	Surface area/(m^2/g)
1	CeO_2	n.d.	n.d.	32
2	10Ni/CeO_2	9.9	n.a.	n.d.
3	10Co/CeO_2	n.a.	9.5	n.d.
4	10NiCo/CeO_2	5.6	5.6	28
5	10NiCo/CeO_2[a]	4.4	4.4	n.d.

[a] the sample was measured after 5 runs; n.a.: not applicable; n.d.: not determined.

(Figure S1), as the darker zones are not necessarily corresponding to Ni or Co domains.

Analysis by STEM coupled with EDX mapping was more informative as it allows identifying the elemental composition within the image (Fig. 2). The large green domains in Fig. 2A and 3B indicate the presence of Ni-containing nanoparticles on CeO_2. Based on the XRD data (Fig. 1A), these domains are identified as large NiO nanoparticles (mainly around 100 nm, with some smaller particles, see Fig. 2A) in the sample before reduction (10Ni/CeO_2-C), and to large domains of metallic Ni (around 75 nm, Fig. 2B) after the sample was reduced (10Ni/CeO_2). For the monometallic material prepared by supporting Co on CeO_2 and prior to reduction (10Co/CeO_2-C), the Co_3O_4 identified by XRD (Fig. 1A) was found to be better dispersed on the CeO_2 support (Fig. 2C) compared to NiO on CeO_2. The 10Co/CeO_2 material obtained upon reduction showed nearly homogeneously dispersed Co species (Fig. 2D), which indicates that the particle size of Co is lower than the detection limit of EDX-mapping (around 30 nm). The relatively small size of the Co nanoparticles is also in agreement with the absence of any signal due to metallic Co in the XRD pattern of 10Co/CeO_2 (Fig. 1B), which suggests a strong metal-support interaction between Co and CeO_2 [4,33,35,45,46,48].

STEM and EDX-mapping of the Ni-Co bimetallic material prior to reduction (10NiCo/CeO_2-C), showed that both Ni and Co are nearly homogeneously dispersed on the CeO_2 surface (Fig. 4 A–D). This demonstrates that the presence of Co prevents the aggregation of Ni species, in contrast to the large domains observed in 10Ni/CeO_2-C. After reduction at 400 °C under H_2, Ni and Co still preserve very good dispersion, with no large metal particles (i.e. > 30 nm) being visible (Fig. 3H). The strong interaction between Co and the CeO_2 support, which promotes the observed high dispersion of both Co and Ni on the surface, has been shown to be related to the formation of a thin layer of reduced CeO_x at the interface with the metallic Co [35]. Based on our results, we infer that this feature prevents Ni from forming large particles in the process of calcination and reduction [33,35,46].

The reducibility of Ni, Co and Ni-Co supported on CeO_2 was further investigated by H_2-TPR (Fig. 4). The support, CeO_2, exhibited two dominant peaks centred at 490 °C (from 300 to 550 °C) and 880 °C (from 700 to above 900 °C), which are attributed to the reduction of surface ceria and bulk ceria, respectively [35,49]. Besides the reduction peaks of CeO_2 at 420 and 815 °C, which are slightly shifted to lower temperature, the monometallic 10Ni/CeO_2-C displays two peaks at

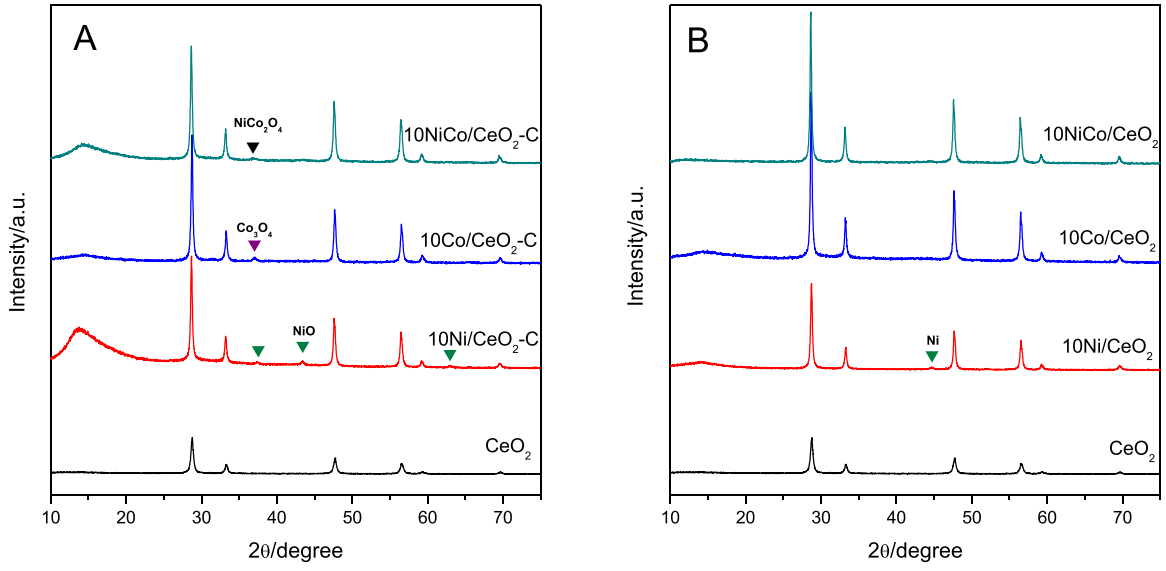

Fig. 1. XRD patterns of calcined CeO_2 and Ni, Co and Ni-Co catalysts supported on CeO_2 before (A) and after reduction (B).

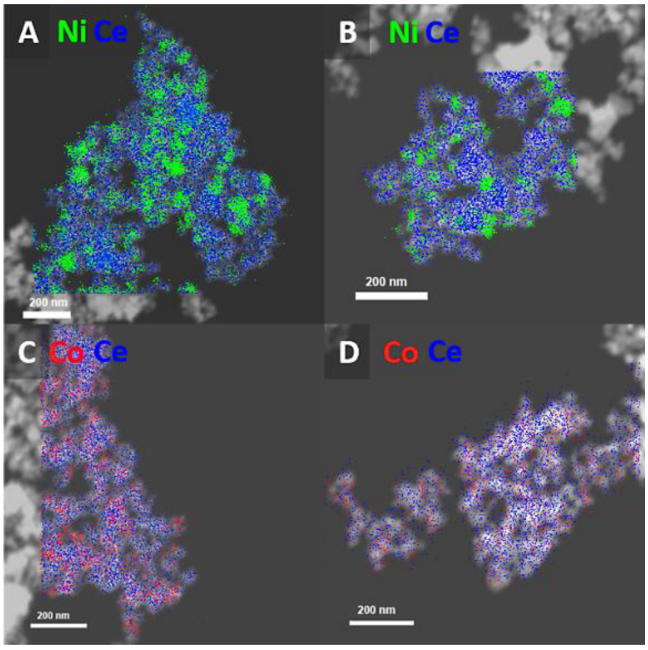

Fig. 2. EDX-mapping coupled with STEM (dark field) pictures of monometallic Ni and Co catalysts supported on CeO_2 before and after reduction. (A) 10Ni/CeO_2-C, (B) 10Ni/CeO_2, (C) 10Co/CeO_2-C, (D) 10Co/CeO_2. The green, red and blue dots represent Ni, Co and Ce, respectively (For interpretation of the references to colour in this figure legend, the reader is referred to the web version of this article.).

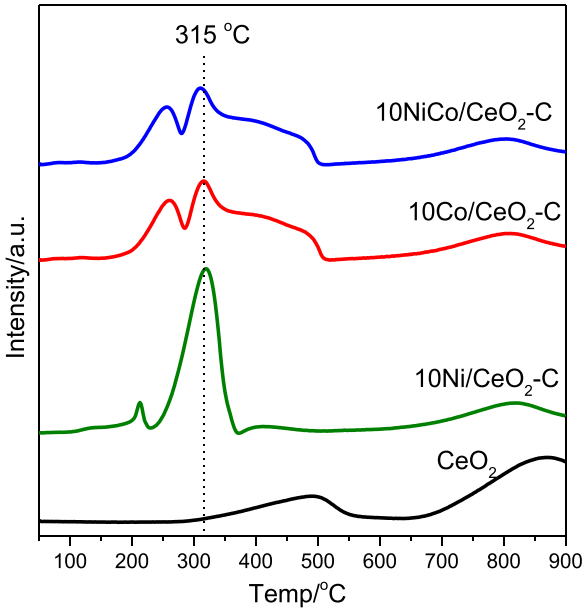

Fig. 4. H_2-TPR profiles of calcined CeO_2 and Ni, Co and Ni-Co catalysts supported on CeO_2.

213 °C (minor) and 320 °C (dominant), which are attributed to the reduction of adsorbed oxygen and NiO, respectively [35,50]. The monometallic 10Co/CeO_2-C showed two main peaks at 260 and 315 °C, which are attributed to the two-step reduction $Co_3O_4 \rightarrow CoO \rightarrow Co$ [51,52]. The large and broad shoulder extending from 350 to 500 °C is probably due the reduction of surface CeO_2. Compared to the monometallic Ni catalyst, the significant increase of the intensity of the reduction peak of surface CeO_2 in the monometallic Co catalyst supports the existence of a strong metal-support interaction between Co and CeO_2, which is in agreement with the formation of a thin layer of reduced support on the metallic Co surface reported in the literature [35,48]. The 10NiCo/CeO_2-C material showed almost identical profile as the one of 10Co/CeO_2-C, with all the peaks shifted by ca. 5 °C to lower temperature. This suggests that, in the bimetallic Ni-Co catalyst, the reduction behaviour is mainly dictated by the presence of Co, including the strong metal-support interaction indicated by the broad shoulder between 350 and 500 °C. This result explains the observed

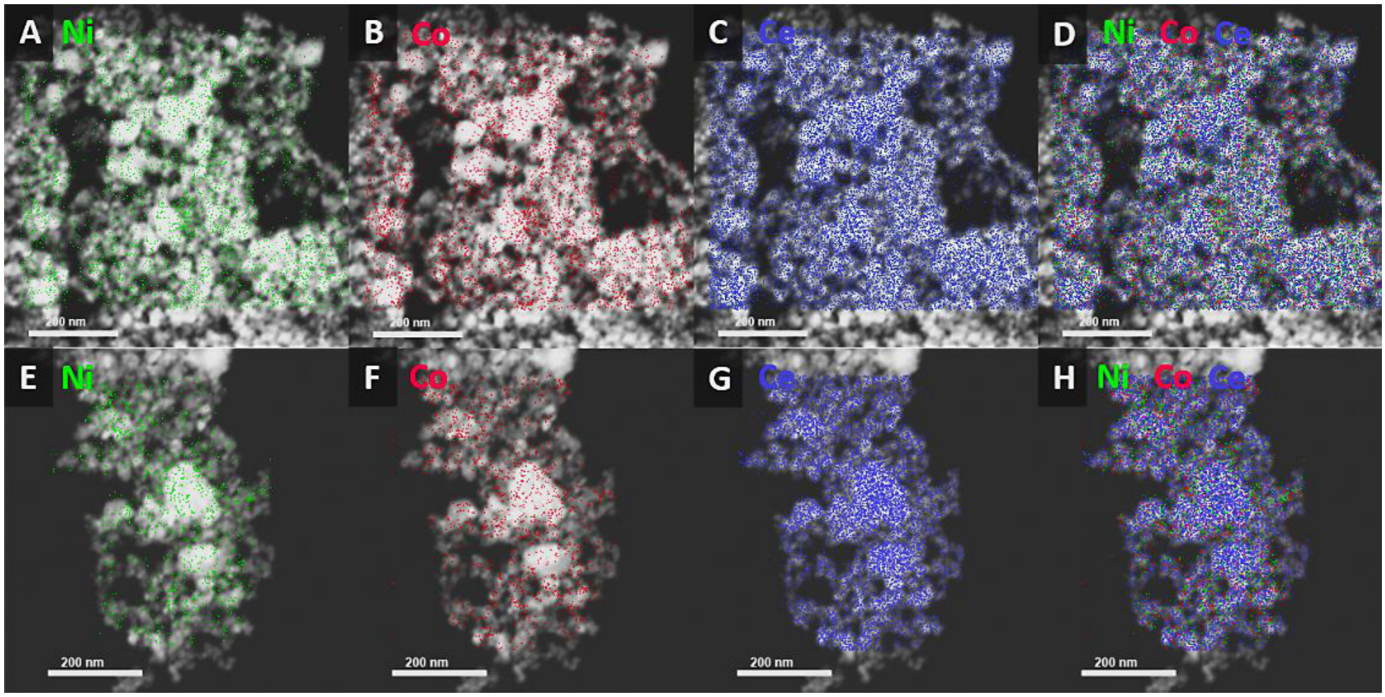

Fig. 3. EDX-mapping coupled with STEM (dark field) pictures of bimetallic Ni-Co catalysts supported on CeO_2 before and after reduction. (A–D) 10NiCo/CeO_2-C, (E–H) 10NiCo/CeO_2. The green, red and blue dots represent Ni, Co and Ce, respectively (For interpretation of the references to colour in this figure legend, the reader is referred to the web version of this article.).

much better dispersion of the metal species in the bimetallic Ni-Co catalyst compared to the monometallic Ni catalyst (Figs. 2 and 4) [35].

The characterisation by EDX-mapping and H_2-TPR indicates a geometrical effect of the presence of Co on the dispersion of Ni on the CeO_2 support. To investigate further the interaction between Co, Ni and the support, selected catalysts were analysed by XPS (Figure S2-4). The XPS signal of the Ni $2p_{3/2}$ core level region of the unreduced 5Ni/CeO_2-C catalyst was deconvoluted into 3 main peaks: at 853.6 eV, assigned to NiO; at 855.6 eV, attributed to $Ni(OH)_2$ and/or NiO(OH); and a satellite peak at 860.6 eV [53–56]. Similar peaks were identified by deconvoluting the Ni $2p_{3/2}$ signal of the unreduced 10NiCo/CeO_2-C catalyst (Figure S2.A and B). After reduction (Figure S2.C and D), in addition to the 3 peaks mentioned above, the deconvolution allowed identifying a peak ascribed to Ni^0 (at 852.3 eV) in catalysts 5Ni/CeO_2 and 10 NiCo/CeO_2 [54,55,57]. These data confirm the successful reduction to metallic Ni. The fact that the majority of the XPS signal stems from oxidised Ni species can be explained considering that XPS is a surface technique (information from the top 1–10 nm of the material) and that the surface of the particles is expected to tend to oxidise in contact with air and moisture [58,59]. The XPS signal of the Co $2p_{3/2}$ core level region of the unreduced 5Co/CeO_2-C catalysts was deconvoluted into 3 main peaks: at 779.5 eV, assigned to cobalt oxides (CoO and/or Co_3O_4); at 781.5 eV, ascribed to $Co(OH)_2$; and a satellite peak at 785.5 eV [55,60,61]. Analogous peaks were identified by deconvoluting the Co $2p_{3/2}$ signal of the unreduced 10NiCo/CeO_2-C catalyst (Figure S3.A and B). After reduction (Figure S3.C and D), in addition to the 3 peaks mentioned above, the deconvolution showed a peak assigned to Co^0 (at 778.0 eV) in the catalysts 5Co/CeO_2 and 10 NiCo/CeO_2 [55,62]. Similarly to what discussed in the case of the supported Ni particles, the presence of oxidised Co species in the reduced samples is attributed to the formation of a layer of oxides and hydroxides at the surface of the particles, generated by contact with air and moisture. The features of the XPS signal of the Ce 3d core level region support the anticipated strong interaction between Co and CeO_2 (Figure S4). This is indicated by the surface reduction of Ce^{4+} and the increase in Ce^{3+} observed in the XPS spectra of the Co-containing catalysts (whereas this effect is absent in the spectra of the catalysts containing Ni but no Co). This matches well with the literature and with our H_2-TPR results [35,52,54]. The XPS data are not conclusive on possible synergistic electronic effects between Ni and Co. Therefore, we infer that the main reason for the improved catalytic performance of bimetallic 10NiCo/CeO_2 is the smaller size and better dispersion of the Ni-containing particles.

3.3. Optimisation of the performance of catalyst 10NiCo/CeO_2

Based on this characterisation study, the optimum activity observed with the bimetallic 10NiCo/CeO_2 catalyst is attributed to presence of the more active Ni compared to the monometallic 10Co/CeO_2, and to the better dispersion of the active metallic species compared to the monometallic 10Ni/CeO_2 catalyst. To further confirm the nature of the active sites, unreduced Ni, Co and bimetallic Ni-Co catalysts were tested under the same conditions employed for the reduced catalysts (Table S1). In the unreduced materials, the metal oxides (NiO, Co_3O_4 and $NiCo_2O_4$) would be the catalytic sites rather than the metallic sites. All the unreduced catalysts had significantly lower activity compared to the reduced ones (Table 1 and 2), with the conversion of glycerol being < 16% in all cases. These results confirm that the metallic sites are the active site in this transfer hydrogenation reaction between glycerol and cyclohexene, in agreement with what shown in the literature [27–29].

The Ni, Co and Ni-Co catalysts with different loading (2, 5 and 10 wt %) supported on CeO_2 were tested to gain better understanding on the effect of the Ni and Co composition (Fig. 5). With the Ni/CeO_2 catalysts, the conversion of glycerol increased with the metal loading up to 5 wt% Ni, at which it reached 55%, whereas it remained nearly constant upon further increase to 10 wt % of Ni. This trend is completely different from the one observed with the Co/CeO_2 and NiCo/CeO_2 catalysts, for which the glycerol conversion and the lactic acid yield exhibited an increasing trend with the increase in metal loading (Fig. 5A). The performance of these catalysts can be analysed also in terms of turnover number (TON) (Fig. 5B). These data show that the TON is nearly constant as a function of metal loading for the monometallic Co-catalysts, whereas an increasing loading of Ni causes a gradual decrease in TON, which is more marked for the monometallic Ni-catalysts compared to the bimetallic Ni-Co materials. These trends are in agreement with the tendency of Ni to form large particles at high loading (see Fig. 3.A–B), which implies that a smaller fraction of the metal is available to act as active site, thus leading to the observed lower TON. On the other hand, Co maintains small metallic domains on the CeO_2 surface also at 10 wt % metal loading (Fig. 2.C–D), thus enabling to have a nearly constant TON as a function of metal loading. The highest TON was observed for 2Ni/CeO_2 and 2NiCo/CeO_2, whereas among the catalysts with 10 wt% metal loading, the highest TON was found for 10NiCo/CeO_2, despite the decrease compared to the 2 wt% material. This confirms the higher intrinsic activity of Ni compared to Co in catalysing the dehydrogenative oxidation of glycerol. Non-noble metal catalysts are generally used with high loading to give high productivity. Indeed, when the catalytic performance is compared in terms of productivity (Fig. 5C) the highest value among the tested catalysts is obtained with the material with the highest TON among those with 10 wt% metal loading, i.e. 10NiCo/CeO_2. This underlines the benefit of the presence of Co in combination with Ni on the catalytic performance [33–35,44,48].

The 5NiCo/CeO_2 catalyst, which achieved intermediate glycerol conversion at 160 °C, was selected for investigating the effect of the reaction temperature (in the range 140 to 200 °C, Figure S2). The conversion of glycerol increased with higher reaction temperature, from 11% (at 140 °C) to 99% (at 200 °C), while the selectivity to lactic acid remained > 98%. The selectivity towards the transfer hydrogenation was steady at around 25% in all range of temperatures. It should be noted that, when only NaOH was used in the reaction system, the conversion of glycerol was rather low, though it increased from 1.6 to 16% (from 140 to 200 °C, Figure S5). This demonstrates the need for a heterogeneous catalyst to carry out the dehydrogenation reaction in this range of relatively mild temperatures [30,31].

To further investigate the effects of the catalyst amount on this reaction, different weights of catalyst (from 0.025 to 0.15 g) were used, while all other parameters were kept constant. The results show a gradual increase in the conversion of glycerol from 29% to > 99.9% upon increase of the loading of the 10NiCo/CeO_2 catalyst (Figure S6).

The role of NaOH was studied in more detail by varying the molar ratio between NaOH and glycerol (from 0 to 2, Figure S7). Without the addition of NaOH, both the conversion of glycerol and the selectivity to lactic acid were very low (conversion of glycerol = 3.5%). If the molar ratio between NaOH and glycerol was increased, the conversion of glycerol gradually increased reaching 91% with 85% yield of lactic acid salt at NaOH/glycerol = 1.5. However, a further increase in the NaOH/glycerol molar ratio to 2 caused a decrease in the conversion of glycerol to 81%, thus indicating that the employed ratio (1.5) is the optimum value. These results confirm that the presence of a base like NaOH in the reaction mixture is critical to induce the deprotonation of one of the hydroxyl groups of glycerol, thus promoting the dehydrogenation of glycerol [21,28]. Moreover, NaOH can catalyse the isomerisation of glyceraldehyde and dihydroxyacetone and lead to the formation of sodium lactate with very high selectivity.

The reaction profile as a function of the reaction time was studied with the 10NiCo/CeO_2 catalyst (Figure S8). The conversion of glycerol increased almost linearly within the first 4.5 h, corresponding to a productivity of lactic acid of 17.4 $g_{(LA)}/(g_{(metal)}h)$. After 6.5 h of reaction, almost complete glycerol conversion (97%) was achieved, with 93% lactic acid (salt) yield. The selectivity towards lactic acid stayed always above 90% and the total selectivity towards by-products

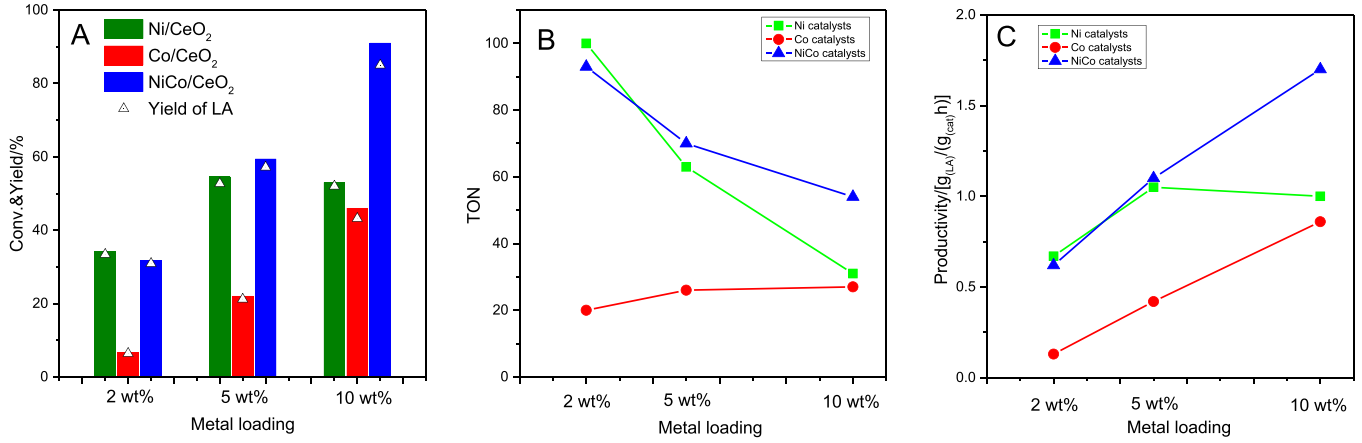

Fig. 5. Catalytic performance of Ni, Co and bimetallic Ni-Co catalysts as a function of the metal loading supported on CeO_2: (A) Glycerol conversion and lactic acid yield; (B) TON: turnover number, defined as the total number of glycerol molecules converted per each metal atom; (C) Productivity, defined as the total mass of lactic acid produced per gram of heterogeneous catalyst per hour. Reaction conditions: aqueous glycerol solution: 10 mmol (0.5 M, 20 mL); cyclohexene: 20 mmol; catalyst: 0.1 g; NaOH: 15 mmol; temperature: 160 °C; reaction time: 4.5 h; N_2 pressure: 20 bar.

(glyceric acid, glycolic acid and propanediol) was around 4%. The selectivity towards the transfer hydrogenation slightly decreased with the reaction time, from 31% to 26%. These results suggest that under the employed reaction conditions the dehydrogenation of glycerol is the rate-determining step, and that once the dihydroxyacetone and/or glyceraldehyde formed, they would be transformed into lactic acid (salt) in a very fast and selective way.

Catalyst $10NiCo/CeO_2$ was also selected for a reusability test (Fig. 6). The fresh catalyst showed 91% conversion of glycerol and 85% yield to lactic acid, while recycling after straightforward washing and drying led to a slight, gradual decrease in activity. After 5 runs, the conversion of glycerol decreased to 73%, while the selectivity towards lactic acid remained unaltered (> 94%). Meanwhile, the selectivity in the transfer hydrogenation gradually increased from 24 to 28% between the first and the fifth run. The gradual loss of activity is probably caused by the leaching of a small fraction of the active components in the alkaline hydrothermal reaction system, since the loading of Ni and Co decreased from 5.6 wt% (each) in the fresh catalyst to 4.4 wt% (each) after 5 runs (entry 5, Table 3).

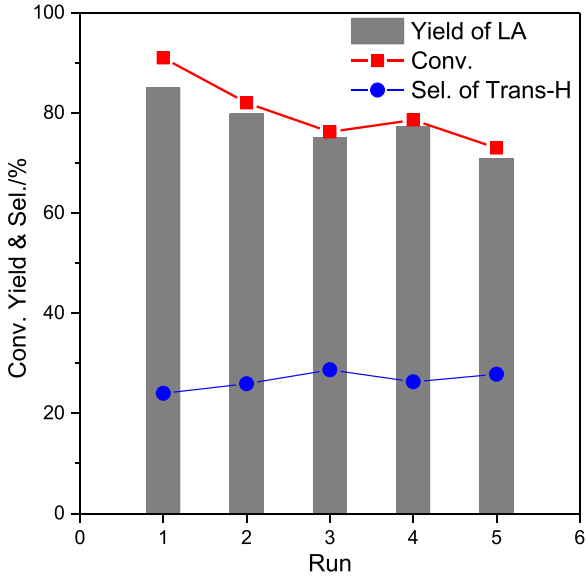

Fig. 6. Reusability test of the $10NiCo/CeO_2$ catalyst for the conversion of glycerol and transfer hydrogenation. Reaction conditions: aqueous glycerol solution: 10 mmol (0.5 M, 20 mL); cyclohexene: 20 mmol; catalyst: 0.1 g; NaOH: 15 mmol; temperature: 160 °C; N_2 pressure: 20 bar.

3.4. Substrate scope for the transfer hydrogenation reaction from glycerol

During the optimisation of the Ni-based catalyst presented above, cyclohexene was employed as hydrogen acceptor in the transfer hydrogenation reaction from glycerol. To expand the scope of applicability of the transfer hydrogenation, we tested a set of H_2 acceptors with different features (a biobased compound as levulinic acid, an aromatic compound as benzene, a compound containing both an aromatic ring and another reducible group as nitrobenzene and a linear, terminal alkene as 1-decene). While cyclohexene and 1-decene were selected as model compounds, the hydrogenation of benzene, nitrobenzene and levulinic acid is of potential industrial relevance [63–69]. The tests were carried out with a 1:1 molar ratio between glycerol and the hydrogen acceptor, at 160 °C under N_2 atmosphere (Scheme 2 and Table 4).

When levulinic acid was employed as the H_2 acceptor, two main products were observed: 4-hydroxypentanoic acid (27% yield), obtained by hydrogenation of the carbonyl group of levulinic acid, and γ-valerolactone (48% yield), obtained by subsequent dehydration (Scheme 2 and entry 1 in Table 4). γ-Valerolactone can be used as food additive, solvent and precursor for polymers [6,68,70,71]. This reaction also gave an 86% yield of lactic acid at 87% glycerol conversion with a very good 88% selectivity in the transfer hydrogenation.

When benzene was tested as H_2 acceptor, a very high selectivity (97%) in the transfer hydrogenation from glycerol was observed, with cyclohexane being the only product (corresponding to complete reduction of benzene). The reduction of benzene is the industrial route for the production of cyclohexane, which is employed as precursor in the synthesis of adipic acid used in the manufacturing of nylon [72,73]. The yield achieved here (25%) is promising considering that under the employed reaction conditions (1:1 molar ratio between glycerol and benzene), the maximum theoretical yield of cyclohexane is 33%. These results were coupled with 79% conversion of glycerol and 77% yield of lactic acid (entry 2, Table 4).

When nitrobenzene was employed as hydrogen acceptor, the reduction of the nitro group is expected to be favoured over the reaction of the aromatic ring. Indeed, the observed products (azoxybenzene with 59% yield, azobenzene with 18% yield and aniline with 7.5% yield) all originate from the reduction of the nitro group (Scheme 2) [63,74–76]. These are all industrially valuable products, with azoxybenzene being utilised in dyes, reducing agents and polymerisation inhibitors; azobenzene being used in dyes, indicators and as additive in polymers; and aniline finding application in producing pesticides, dyes and as the precursor to polyurethane [77–79]. For this reaction, the selectivity in

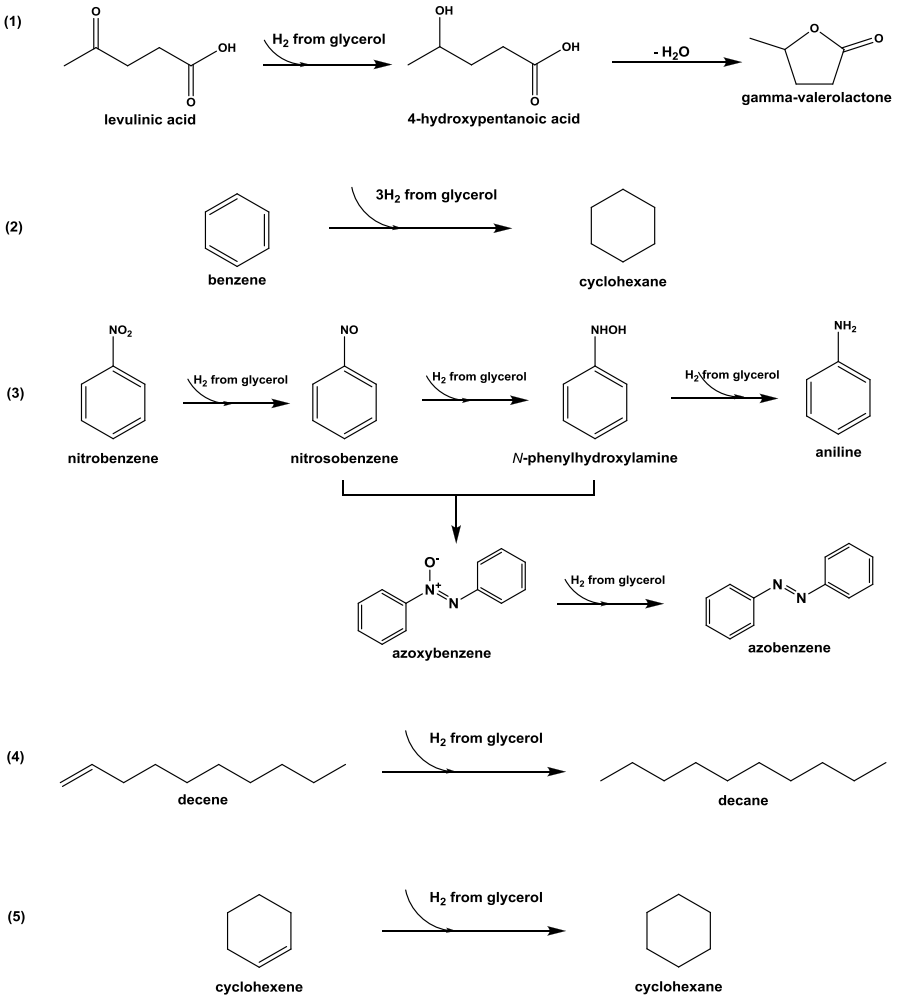

Scheme 2. Reduction routes of various H_2 acceptors.

the transfer hydrogenation from glycerol was > 100%. This can be explained considering the strong oxidative ability of nitrobenzene, which led to the further oxidation of the triose intermediates to glyceric acid and glycolic acid (entry 3, Table 4), similarly to what is generally observed in the oxidation of glycerol in the presence of O_2 [25,80–82]. Therefore, glyceric acid (52% yield) becomes the major product under these conditions, with lactic acid being obtained in much lower yield (23%).

When 1-decene was selected as a linear H_2 acceptor with a primary C=C bond, 92% conversion of glycerol and 91% yield of lactic acid was achieved after reaction, while 85% of decene was hydrogenated to decane, corresponding to a remarkably high 94% selectivity in the transfer hydrogenation (entry 4, Table 4). This is much higher than what was found when using cyclohexene as the H_2 acceptor (entry 5,

Table 4
Catalytic performance of 10NiCo/CeO_2 catalysts with different H_2 acceptors.

Entry	H_2 acceptor	Conv.$_{GLY}$ (%)	$S_{(transfer-H)}$ (%)	Yields of products from glycerol (%)			Yields of products from H_2 acceptor (%)[c]		
				Lactic acid	Glyceric acid	Glycolic acid	P1	P2	P3
1	levulinic acid[a]	87	88	86	0.3	0.1	27	48	n.a.
2	benzene	79	97	77	1.1	0	25	n.a.	n.a.
3	nitrobenzene	65	> 100	23	52	11	59	18	7.5
4	1-decene	92	94	91	0	0	85	n.a.	n.a.
5	cyclohexene[b]	91	24	85	0.8	0	11	n.a.	n.a.

Entry 1, P1: 4-hydroxypentanoic acid; P2: γ-valerolactone.
Entry 2, P1: cyclohexane (the maximum theoretical yield of cyclohexane is 33.3%.).
Entry 3, P1: azoxybenzene; P2: azobenzene; P3: aniline.
Entry 4, P1: decane.
Entry 5, P1: cyclohexane (the maximum theoretical yield of cyclohexane is 50%.).
Reaction conditions: aqueous glycerol solution: 10 mmol (0.5 M, 20 mL); H_2 acceptor: 10 mmol; catalyst: 0.1 g; NaOH: 15 mmol; temperature: 160 °C; N_2 pressure: 20 bar.

[a] 25 mmol NaOH was used in the reaction, due to the extra 10 mmol consumption by levulinic acid.
[b] 20 mmol cyclohexene was used in the reaction.
[c] P1-3 represents the main products obtained from the reduction of H_2 acceptors.

Table 4). This result is probably due to the higher accessibility of the C=C bond in a linear alkene with a terminal double bond as 1-decene compared to the more sterically-hindered cyclohexene.

The study of substrate scope for the transfer hydrogenation reaction from glycerol demonstrated that our catalytic system based on 10NiCo/CeO_2 is able to efficiently promote the conversion glycerol to lactic acid while exploiting the liberated hydrogen in the reduction of different unsaturated compounds to achieve the synthesis of useful target products without requiring an external H_2 source.

4. Conclusions

Bimetallic Ni-Co catalysts supported on CeO_2 were prepared and tested for the transfer hydrogenation from glycerol to various unsaturated compounds, in which lactic acid and the corresponding hydrogenated products were obtained in a one-pot batch reaction. Introducing Co into the formulation of the Ni-based catalysts was crucial to prevent the aggregation of Ni into large particles. This was proven by the higher activity of the bimetallic 10NiCo/CeO_2 catalyst compared the Ni- or Co-based counterparts, and by characterisation of the catalytic materials by EDX-mapping and H_2-TPR, which demonstrated the high dispersion of Ni-Co sites on the CeO_2 support. The bimetallic 10NiCo/CeO_2 catalyst exhibited very high activity (91% glycerol conversion) and selectivity to lactic acid (94%) at 160 °C, 4.5 h under N_2 atmosphere in the presence of NaOH as promoter. This result demonstrates that excellent conversion and selectivity can be achieved using a catalyst with a relatively low loading of Ni and Co and that operates at milder reaction conditions compared to other non-noble metal catalysts for glycerol dehydrogenation reactions [20,25–29]. Moreover, various H_2 acceptors (levulinic acid, benzene, nitrobenzene, 1-decene, cyclohexene) were tested in the transfer hydrogenation from glycerol, exploiting *in-situ* the hydrogen liberated in the dehydrogenative oxidation of glycerol to generate several useful products.

Declaration of Competing Interest

The authors declare that they have no known competing financial interests or personal relationships that could have appeared to influence the work reported in this paper.

Acknowledgments

We would like to thank the financial support from the China Scholarship Council for the Ph.D. grant of Zhenchen Tang, the technical support from Leon Rohrbach, Jan Henk Marsman, Erwin Wilbers, Anne Appeldoorn and Marcel de Vries, the TEM-EDX support from Dr. Marc Stuart and the ICP-OES support from Johannes van der Velde. We also acknowledge Dr. Matteo Miola for useful scientific discussion of the XPS data.

Appendix A. Supplementary data

Supplementary material related to this article can be found, in the online version, at doi:https://doi.org/10.1016/j.apcatb.2019.118273.

References

[1] A. Corma, S. Iborra, A. Velty, Chem. Rev. 107 (2007) 2411–2502.
[2] G.W. Huber, S. Iborra, A. Corma, Chem. Rev. 106 (2006) 4044–4098.
[3] M. Besson, P. Gallezot, C. Pinel, Chem. Rev. 114 (2014) 1827–1870.
[4] D.M. Alonso, S.G. Wettstein, J.A. Dumesic, Chem. Soc. Rev. 41 (2012) 8075–8098.
[5] S.A. Kondrat, P.J. Miedziak, M. Douthwaite, G.L. Brett, T.E. Davies, D.J. Morgan, J.K. Edwards, D.W. Knight, C.J. Kiely, S.H. Taylor, ChemSusChem 7 (2014) 1326–1334.
[6] R.A. Sheldon, Green Chem. 16 (2014) 950–963.
[7] Y.-C. Lin, Int. J. Hydrogen Energy 38 (2013) 2678–2700.
[8] C.H. Zhou, J.N. Beltramini, Y.X. Fan, G.Q. Lu, Chem. Soc. Rev. 37 (2008) 527–549.
[9] A. Behr, J. Eilting, K. Irawadi, J. Leschinski, F. Lindner, Green Chem. 10 (2008) 13–30.
[10] T. Ito, Y. Nakashimada, K. Senba, T. Matsui, N. Nishio, J. Biosci. Bioeng. 100 (2005) 260–265.
[11] G.W. Huber, J.W. Shabaker, J.A. Dumesic, Science 300 (2003) 2075–2077.
[12] M. Dusselier, P. Van Wouwe, A. Dewaele, E. Makshina, B.F. Sels, Energy Environ. Sci. 6 (2013) 1415–1442.
[13] Z. Tang, S.L. Fiorilli, H.J. Heeres, P.P. Pescarmona, ACS Sustain. Chem. Eng. 6 (2018) 10923–10933.
[14] H.J. Cho, C.-C. Chang, W. Fan, Green Chem. 16 (2014) 3428–3433.
[15] K.L. Wasewar, A.A. Yawalkar, J.A. Moulijn, V.G. Pangarkar, Ind. Eng. Chem. Res. 43 (2004) 5969–5982.
[16] Y. Wang, Y. Tashiro, K. Sonomoto, J. Biosci. Bioeng. 119 (2015) 10–18.
[17] A. Wawrzetz, B. Peng, A. Hrabar, A. Jentys, A.A. Lemonidou, J.A. Lercher, J. Catal. 269 (2010) 411–420.
[18] W. Lubitz, W. Tumas, Chem. Rev. 107 (2007) 3900–3903.
[19] R.D. Cortright, R.R. Davda, J.A. Dumesic, Nature 418 (2002) 964–967.
[20] H. Yin, H. Yin, A. Wang, L. Shen, J. Ind. Eng. Chem. 57 (2018) 226–235.
[21] Y. Shen, S. Zhang, H. Li, Y. Ren, H. Liu, Chem. Eur. J. 16 (2010) 7368–7371.
[22] R.K.P. Purushothaman, J. van Haveren, D.S. van Es, I. Melián-Cabrera, J.D. Meeldijk, H.J. Heeres, Appl. Catal. B 147 (2014) 92–100.
[23] E. Maris, R. Davis, J. Catal. 249 (2007) 328–337.
[24] F. Auneau, L.S. Arani, M. Besson, L. Djakovitch, C. Michel, F. Delbecq, P. Sautet, C. Pinel, Top. Catal. 55 (2012) 474–479.
[25] T. van Haasterecht, T.W. van Deelen, K.P. de Jong, J.H. Bitter, Catal. Sci. Technol. 4 (2014) 2353–2366.
[26] B.C. Miranda, R.J. Chimentão, J.B.O. Santos, F. Gispert-Guirado, J. Llorca, F. Medina, F.L. Bonillo, J.E. Sueiras, Appl. Catal. B 147 (2014) 464–480.
[27] R. Palacio, S. Torres, D. Lopez, D. Hernandez, Catal. Today 302 (2018) 196–202.
[28] D. Roy, B. Subramaniam, R.V. Chaudhari, ACS Catal. 1 (2011) 548–551.
[29] G. Yang, Y. Ke, H. Ren, C. Liu, R. Yang, W. Dong, Chem. Eng. J. 283 (2016) 759–767.
[30] H. Kishida, F. Jin, Z. Zhou, T. Moriya, H. Enomoto, Chem. Lett. 34 (2005) 1560–1561.
[31] Z. Shen, F. Jin, Y. Zhang, B. Wu, A. Kishita, K. Tohji, H. Kishida, Ind. Eng. Chem. Res. 48 (2009) 8920–8925.
[32] D. Formenti, F. Ferretti, F.K. Scharnagl, M. Beller, Chem. Rev. (2018), https://doi.org/10.1021/acs.chemrev.8b00547.
[33] S. De, J. Zhang, R. Luque, N. Yan, Energy Environ. Sci. 9 (2016) 3314–3347.
[34] V.M. Gonzalez-delaCruz, R. Pereñiguez, F. Ternero, J.P. Holgado, A. Caballero, J. Phys. Chem. C 116 (2012) 2919–2926.
[35] H. Ay, D. Üner, Appl. Catal. B 179 (2015) 128–138.
[36] A. Movasati, S.M. Alavi, G. Mazloom, Fuel 236 (2019) 1254–1262.
[37] P. Lakshmanan, P.P. Upare, N.-T. Le, Y.K. Hwang, D.W. Hwang, U.H. Lee, H.R. Kim, J.-S. Chang, Appl. Catal. A 468 (2013) 260–268.
[38] J. Feng, W. Xiong, B. Xu, W. Jiang, J. Wang, H. Chen, Catal. Commun. 46 (2014) 98–102.
[39] F. Mauriello, H. Ariga, M.G. Musolino, R. Pietropaolo, S. Takakusagi, K. Asakura, Appl. Catal. B 166-167 (2015) 121–131.
[40] D. Roy, B. Subramaniam, R.V. Chaudhari, Catal. Today 156 (2010) 31–37.
[41] O. Arbeláez, T.R. Reina, S. Ivanova, F. Bustamante, A.L. Villa, M.A. Centeno, J.A. Odriozola, Appl. Catal. A 497 (2015) 1–9.
[42] R.L. Manfro, T.P.M.D. Pires, N.F.P. Ribeiro, M.M.V.M. Souza, Catal. Sci. Technol. 3 (2013) 1278–1287.
[43] R. Pérez-Hernández, G. Mondragón Galicia, D. Mendoza Anaya, J. Palacios, C. Angeles-Chavez, J. Arenas-Alatorre, Int. J. Hydrogen Energy 33 (2008) 4569–4576.
[44] P. Djinović, I.G. Osojnik Črnivec, B. Erjavec, A. Pintar, Appl. Catal. B 125 (2012) 259–270.
[45] Z. Bian, S. Das, M.H. Wai, P. Hongmanorom, S. Kawi, ChemPhysChem 18 (2017) 3117–3134.
[46] L. Chen, Q. Zhu, Z. Hao, T. Zhang, Z. Xie, Int. J. Hydrogen Energy 35 (2010) 8494–8502.
[47] J. Zhang, H. Wang, A.K. Dalai, J. Catal. 249 (2007) 300–310.
[48] S. Kawi, Y. Kathiraser, J. Ni, U. Oemar, Z. Li, E.T. Saw, ChemSusChem 8 (2015) 3556–3575.
[49] F. Giordano, A. Trovarelli, C. de Leitenburg, M. Giona, J. Catal. 193 (2000) 273–282.
[50] S. Xu, X. Yan, X. Wang, Fuel 85 (2006) 2243–2247.
[51] S.M. de Lima, A.M. da Silva, L.O.O. da Costa, U.M. Graham, G. Jacobs, B.H. Davis, L.V. Mattos, F.B. Noronha, J. Catal. 268 (2009) 268–281.
[52] L.F. Liotta, G. Di Carlo, G. Pantaleo, A.M. Venezia, G. Deganello, Appl. Catal. B 66 (2006) 217–227.
[53] J. Lin, C. Ma, Q. Wang, Y. Xu, G. Ma, J. Wang, H. Wang, C. Dong, C. Zhang, M. Ding, Appl. Catal. B 243 (2019) 262–272.
[54] G. Zhou, H. Liu, K. Cui, A. Jia, G. Hu, Z. Jiao, Y. Liu, X. Zhang, Appl. Surf. Sci. 383 (2016) 248–252.
[55] N.S. McIntyre, M.G. Cook, Anal. Chem. 47 (1975) 2208–2213.
[56] W. Yang, X. Yang, C. Hou, B. Li, H. Gao, J. Lin, X. Luo, Appl. Catal. B 259 (2019) 118020.
[57] S. Somacescu, N. Cioatera, P. Osiceanu, J.M. Calderon-Moreno, C. Ghica, F. Neaţu, M. Florea, Appl. Catal. B 241 (2019) 393–406.
[58] H. Cheng, Y.-Z. Su, P.-Y. Kuang, G.-F. Chen, Z.-Q. Liu, J. Mater. Chem. A 3 (2015) 19314–19321.
[59] X. Sheng, B. Wouters, T. Breugelmans, A. Hubin, I.F.J. Vankelecom, P.P. Pescarmona, Appl. Catal. B 147 (2014) 330–339.
[60] N.S. McIntyre, D.D. Johnston, L.L. Coatsworth, R.D. Davidson, J.R. Brown, Surf.

Interface Anal. 15 (1990) 265–272.
[61] S. Li, Y. Wang, L. Gao, Y. Wu, X. Yang, P. Sheng, G. Xiao, Microporous Mesoporous Mater. 262 (2018) 154–165.
[62] S. Gupta, N. Patel, R. Fernandes, R. Kadrekar, A. Dashora, A.K. Yadav, D. Bhattacharyya, S.N. Jha, A. Miotello, D.C. Kothari, Appl. Catal. B 192 (2016) 126–133.
[63] D. Tavor, I. Gefen, C. Dlugy, A. Wolfson, Synth. Commun. 41 (2011) 3409–3416.
[64] Z. Mahimwalla, K.G. Yager, J.-i. Mamiya, A. Shishido, A. Priimagi, C.J. Barrett, Polym. Bull. 69 (2012) 967–1006.
[65] P. Liu, H. Xie, S. Tan, K. You, N. Wang, H.J.R.K. Luo, C. Letters, React. Kinet. Catal. Lett. 97 (2009) 101–108.
[66] K.M. Bratlie, H. Lee, K. Komvopoulos, P. Yang, G.A. Somorjai, Nano Lett. 7 (2007) 3097–3101.
[67] Z.-p. Yan, L. Lin, S. Liu, Energy Fuels 23 (2009) 3853–3858.
[68] J.C. Serrano-Ruiz, R. Luque, A. Sepulveda-Escribano, Chem. Soc. Rev. 40 (2011) 5266–5281.
[69] W. Luo, M. Sankar, A.M. Beale, Q. He, C.J. Kiely, P.C.A. Bruijnincx, B.M. Weckhuysen, Nat. Commun. 6 (2015) 6540.
[70] K. Hengst, M. Schubert, H.W.P. Carvalho, C. Lu, W. Kleist, J.-D. Grunwaldt, Appl. Catal. A 502 (2015) 18–26.
[71] A.S. Piskun, J. Ftouni, Z. Tang, B.M. Weckhuysen, P.C.A. Bruijnincx, H.J. Heeres, Appl. Catal. A 549 (2018) 197–206.
[72] M. Dugal, G. Sankar, R. Raja, J.M. Thomas, Angew. Chem. Int. Ed. 39 (2000) 2310–2313.
[73] U. Schuchardt, D. Cardoso, R. Sercheli, R. Pereira, R.S. da Cruz, M.C. Guerreiro, D. Mandelli, E.V. Spinacé, E.L. Pires, Appl. Catal. A 211 (2001) 1–17.
[74] X. Cui, C. Zhang, F. Shi, Y. Deng, Chem. Commun. 48 (2012) 9391–9393.
[75] B. Zhou, J. Song, H. Zhou, L. Wu, T. Wu, Z. Liu, B. Han, RSC Adv. 5 (2015) 36347–36352.
[76] A. Wolfson, C. Dlugy, Y. Shotland, D. Tavor, Tetrahedron Lett. 50 (2009) 5951–5953.
[77] G.D. Yadav, R.K. Mewada, Chem. Eng. J. 221 (2013) 500–511.
[78] N. Daems, J. Wouters, C. Van Goethem, K. Baert, C. Poleunis, A. Delcorte, A. Hubin, I.F.J. Vankelecom, P.P. Pescarmona, Appl. Catal. B 226 (2018) 509–522.
[79] N. Daems, F. Risplendi, K. Baert, A. Hubin, I.F.J. Vankelecom, G. Cicero, P.P. Pescarmona, J. Mater. Chem. A 6 (2018) 13397–13411.
[80] A. Tsuji, K.T. Rao, S. Nishimura, A. Takagaki, K. Ebitani, ChemSusChem 4 (2011) 542–548.
[81] M. Sankar, N. Dimitratos, D.W. Knight, A.F. Carley, R. Tiruvalam, C.J. Kiely, D. Thomas, G.J. Hutchings, ChemSusChem 2 (2009) 1145–1151.
[82] J. Xu, H. Zhang, Y. Zhao, B. Yu, S. Chen, Y. Li, L. Hao, Z. Liu, Green Chem. 15 (2013) 1520–1525.